Numerical simulation of the flow around the keel of a yacht

Renata M. B. Chaves*

Mariana F. O. F. Lima**

Alexandre Teixeira P. Alho**
**Departamento de Engenharia Naval e Oceanica
Universidade Federal do Rio de Janeiro

Atila P. Silva Freire*
*Programa de Engenharia Mecânica, COPPE/UFRJ
C.P. 68503, 21945-970, Rio de Janeiro, Brasil

Abstract. *In a companion paper, the hot-wire anemometry technique was used to characterize the flow around a typical keel of modern racing yachts. The experiments were conducted in a low speed wind tunnel in one downstream station. The present work discusses the applicability of different turbulent models for the adequate description of the flow around the keel. A turbulence model based on the eddy-viscosity assumption and a Reynolds Stress Model were used. All data were compared with the experiments performed through the hot-wire anemometry measurements.*

Keywords: *yacht design, keel, hot-wire anemometry.*

1. Introduction

In a companion paper, the present authors have already stressed the large number of applications that juncture flows have in technology and nature. External aerodynamics, turbomachinery, flows over buildings, electronic component cooling, animal flight and swimming, all these problems involve multibody geometries that are prone to flow separation and wake interactions.

The major consequence is that only full three-dimensional treatments of the problem will be capable of unveiling the relevant physics associated to the complexities of horseshoe vortex systems and wake interactions. In turbulence, we remind the reader that this single feature will impose difficult conditions for the numerical simulation of the flow. The necessary restrictions caused by a limited grid size allowance are bound to prevent faithful descriptions of the problem.

A typical characteristic of juncture flows is the mean secondary flow structure known as the horseshoe vortex. This vortical structure results from two combined effects: the skewing and stretching of the transverse vorticity present in a boundary layer that is formed on a wall, and the rolling up of the incoming fluid due large adverse pressure gradients. Thus, the turbulent flow around an appendage-body junction is a very complex, highly three dimensional flow.

Most of the research presented in literature to study junction flows deals with cylinders mounted onto a flat plate, frequently at a zero angle of attack. For yacht design applications, however, this condition is very restrictive. The hull of a yacht in sailing conditions always attains angles of attack different from zero with the main flow. More than that, these operational conditions impose complexes flows around the keel of the yacht.

The purpose of this work in to perform an investigation of the flow around a typical keel of a modern racing yacht from a numerical point of view. In fact, as mentioned before, the present work is complementary to a companion paper where an experimental study of the flow around the same keel was conducted through the hot-wire anemometry measurements. In this sense, the contribution will be extensive. Since the bulb of keel is a body of revolution, the interaction that takes place at the junction region between the several complex flow elements described above is possibly very different from the interactions that take place on a flat wall. Thus, with the present two works, we do intend two things: i) to provide the reader with a detailed experimental characterization of the flow field and, ii) to assess the usefulness of the available turbulence models to predict such a flow.

The paper will present numerical simulations obtained through models based on the eddy viscosity concept and models that rely on a direct modeling of the Reynolds stress (RSM). These models are supposed to be sophisticated enough to furnish good representations of the problem.

Despite all this complexity, algebraic isotropic eddy viscosity models and mixing length models still continue to be used to predict junction flows. These models are known to produce acceptable mean velocity results for boundary layers away from adverse pressure gradient regions and separation. In the aeronautical industry, for example, the Baldwin-Lomax model has been widely used. The $\kappa-\varepsilon$ model has also been used extensively. Reynolds stress models, on the other hand, have been used more timidly. The renormalization group version of the $\kappa-\varepsilon$ model provides reasonable predictions of the turbulent kinetic energy. All models, however, underpredict the vortex strength. Davenport and Simpson (1992) tested six different models and concluded that the Cebeci-Smith algebraic model and an algebraic stress model were the models to give the best results for the calculation of the shearing stress around a junction; the $\kappa-\varepsilon$ performed poorly. Ölçmen and Simpson (1996, 1997) also tested seven further second-order turbulence models against their set of data. They found that none of them captured the high Reynolds-averaged double and triple fluctuating

products. Parneix et al. (1998) applied the V2F model to junction flows. The calculated separation lines compared well with those obtained by flow visualization. The production of turbulence near the obstacle was better predicted than with the κ–ε model.

The control of horseshoe vortices was extensively examined by Barberis et al. (1998). Basically two methods were studied: i) the modification of pressure field induced by the obstacle by changing its geometry with a strake, and ii)the implementation of suction through a hole located near the separation line. The study was experimental, and was conducted in a subsonic wind tunnel. The surface flow properties were characterized by using a viscous coating to allow a visualization of the skin friction line patterns. Quantitative results were obtained with Laser Doppler Velocimetry (LDV). The paper showed that the geometrical extent of the separation region is reduced and the separation line is much close to the leading edge when a strake is fitted to the model. Using active control, that is, producing suction through a hole located in the plane of symmetry in front of the leading edge of the obstacle, the vortex size is reduced and its location displaced towards the origin of the obstacle.

A two-equation model and a near-wall second-moment closure were used by Deng and Visonneau (1998) to compute junction flow. The Reynolds stress model captured the anisotropic behavior of the normal Reynolds stresses and the amplification of longitudinal velocity. The anisotropy also provoked strong values of shearing stress near the wall. The high mean kinetic energy levels in front of the nose were not well simulated.

Non-linear eddy viscosity and algebraic stress models can provide a link between linear eddy viscosity models and the full differential Reynolds stress model. Gatski and Jongen (2000) reviewed several models providing a perspective view on their various similarities and differences. Their link with Reynolds stress models and the best predictive capability over standard linear eddy viscosity models was also addressed.

The subject of junction flows received a thorough review by Simpson (2001). The author discussed the physics of flow separation at junctions for both laminar and turbulent flows. The three-dimensional separation with resulting horseshoe vortices that are generated at junctions were explained in phenomenological terms. Calculation flow methods were also reviewed. For that matter, Simpson advices one to use methods that can capture large-scale chaotic vertical motions. Works about the control, modification, or elimination of horseshoe vortices were also reviewed.

Cummings et al. (2003) considered the computational challenges involved in the numerical computation of flows under a high angle of attack. When vertical and massively separated flows occur, appropriate numerical algorithms have to be used. In addition, grids must be created that provide accurate simulations of the flow field. The paper proposes solutions based on hybrid turbulence models.

2. Numerical simulation

2.1 Governing equations

The Navier-Stokes equations are the governing equations for all types of flow regime, including turbulent flow. However, at realistic Reynolds numbers the length and time scales present in the flow span such a large spectrum that any attempt at resolving the flow down the smallest scales results in a sound physical impossibility due to present computer power. To overcome the difficulties imposed by the richness in relevant scales present in the flow, a current practice is to resort to *turbulence models*.

Turbulence models are obtained by modifying the Navier-Stokes equations to introduce averaged and fluctuating quantities. Then, the continuity and the two-dimensional, incompressible Reynolds averaged Navier-Stokes equations reduce to:

$$\frac{\partial \overline{u_i}}{\partial x_i} = 0$$

$$\frac{\partial \overline{u_i}}{\partial t} + u_i \frac{\partial \overline{u}_j}{\partial x_i} = -\frac{1}{\rho}\frac{\partial \overline{p}}{\partial x_i} + \frac{\partial}{\partial x_j}\left(\upsilon \frac{\partial \overline{u_i}}{\partial x_j} + \frac{\partial \overline{u_j}}{\partial x_i} \right) - \frac{\partial}{\partial x_j}\left(\overline{u'_i u'_j} \right)$$

where capital letters are used for the time-averaged quantities and small letters to the fluctuating quantities. The notation is classical. Thus, $u'_i u'_j$ denotes the Reynolds stress.

Turbulence models provide mathematical models for the Reynolds stress. In general compendia in fluid mechanics, these models are basically divided into two classes: eddy viscosity models and Reynolds stress models. In the present work, two turbulence models were chosen for scrutiny, one from each different classification: an eddy viscosity model, the SST κ–ω Based Model and a Reynolds stress model, the BSL RSM. These will be discussed next.

2.2 The SST κ–ω model

Eddy viscosity turbulence models consider that the Reynolds stress can be related to the mean velocity gradients through the rate of strain tensor and an eddy viscosity, so that one can write:

$$-\overline{u_i' u_j'} = \nu_t \left(\frac{\partial \overline{u_i}}{\partial x_j} + \frac{\partial \overline{u_j}}{\partial x_i} \right) - \frac{2}{3} \kappa \delta_{ij}$$

where ν_t denotes the eddy viscosity and δ_{ij} is the Kronecker delta.

In two-equation models, the turbulent viscosity is specified through two transportable characteristic quantities of the flow. These quantities are then to be found from differential equations that must be derived directly from the Reynolds equations. Typical transportable quantities used to specify the turbulent viscosity are the turbulent kinetic energy, κ, the dissipation per unit mass, ε, and, the specific dissipation rate, ω.

The κ–ω model considers that the turbulent viscosity is relater to the turbulent kinetic energy and the turbulent frequency through expression:

$$\mu_\tau = \rho \, (\kappa/\omega)$$

The κ–ω formulation has become very popular over the last few years for its apparent superior performance for the treatment of near wall conditions. The κ–ω model does not require the introduction of the typical non-linear dumping functions present in the κ–ε model and, for this reason, should be more accurate and robust. As a matter of fact, the κ–ω model can be resolved with a near wall resolution of $y^+ < 2$.

The two transport equations for the κ–ω model can be written as:

$$\frac{\partial \kappa}{\partial t} + \overline{u_i} \frac{\partial \kappa}{\partial x_i} = \frac{\partial}{\partial x_i} \left[\left(\upsilon + \left(\frac{\upsilon_t}{\sigma_\kappa} \right) \right) \frac{\partial \kappa}{\partial x_i} \right] + P_k - \beta' \kappa \omega$$

$$\frac{\partial \omega}{\partial t} + \overline{u_i} \frac{\partial \omega}{\partial x_i} = \frac{\partial}{\partial x_i} \left[\left(\upsilon + \left(\frac{\upsilon_t}{\sigma_\omega} \right) \right) \frac{\partial \omega}{\partial x_i} \right] + \alpha \frac{\omega}{k} P_k - \beta \omega^2$$

$$P_k = -\overline{u_i' u_j'} \frac{\partial \overline{u_j}}{\partial x_i}$$

The κ–ω model constants are given by:

$$\alpha = 5/9$$

$$\beta' = 0.09 \qquad \beta = 0.075$$

$$\sigma_{\omega 2} = 2 \qquad \sigma_{\kappa 2} = 2$$

The Shear Stress Transport (SST) κ–ω Model, accounts for turbulent shear stress transport by considering:

$$\upsilon_\tau = \frac{\alpha_1 \kappa}{\max(\alpha_1 \omega, SF_2)}$$

where F_2 is a blending function, and S is an invariant measure of the strain rate.

The blending function F_2 is given by:

$$F_2 = \tanh(\arg_2^2)$$

with:

$$\arg_2 = \max\left(\frac{2\sqrt{k}}{\beta'\omega y}, \frac{500\upsilon}{y^2\omega}\right)$$

2.3 The BSL Reynolds Stress Model

Reynolds Stress Turbulence Models do not use the eddy viscosity hypothesis. Alternatively, the RSM transport equations are solved for each of the six individual stress components.

The Reynolds stress transport equation for ω based models is given by:

$$\frac{\partial \tau_{ij}}{\partial t} + \frac{\partial \bar{u}_k \tau_{ij}}{\partial x_k} = P_{ij} + \frac{2}{3}\beta'\omega\kappa\delta_{ij} - P_{ij} + \frac{\partial}{\partial x_k}\left(\left(\upsilon + \frac{\upsilon_t}{\sigma^*}\right)\frac{\partial \tau_{ij}}{\partial x_k}\right)$$

where the equation for ω is given by:

$$\frac{\partial \omega}{\partial t} + \frac{\partial \bar{u}_k \omega}{\partial x_k} = \alpha_3 \frac{\omega}{\kappa} P_\kappa - \beta_3 \omega^2 + \frac{\partial}{\partial x_k}\left(\left(\upsilon + \frac{\upsilon_t}{\sigma_{\omega 3}}\right)\frac{\partial \omega}{\partial x_k}\right) + (1 - F_1)^2 \frac{1}{\sigma_2 \omega}\frac{\partial \kappa}{\partial x_k}\frac{\partial \omega}{\partial x_k}$$

In the above equation, the BSL blending principle is applied so that the coefficients α and β of the ω-equation are obtained from two distinct sets of constants.

For the ω-discriminated region, the corresponding constants are:

$$\sigma_1^* = 2$$
$$\beta_1 = 0.0750$$
$$k = 0.41$$
$$\alpha_1 = \frac{\beta}{\beta'} - \frac{k^2}{\sigma(\beta')^{0.5}} = 0.553$$

For the ε-discriminated region, the corresponding constants are:

$$\sigma_2^* = 1$$
$$\beta_2 = 0.0828$$
$$k = 0.41$$
$$\alpha = \frac{\beta}{\beta'} - \frac{k^2}{\sigma(\beta')^{0.5}} = 0.440$$

Finally, the blending coefficients are found from a linear interpolation through the relation:

$$\phi_3 = F\,\phi_1 + (1\text{-}F)\,\phi_2$$

where:

$$F = \tanh(\arg^4)$$

with:

$$\arg = \min\left(\max\left(\frac{\sqrt{k}}{\beta'\omega y}, \frac{500\upsilon}{y^2\omega}\right), \frac{4\rho\kappa}{CD_{\kappa\omega}\sigma_{k-\varepsilon}y^2}\right)$$

and:

$$CD_{\kappa\omega} = \max\left(2\rho\frac{1}{\sigma_{\kappa-\varepsilon}\omega}\frac{\partial \kappa}{\partial x_j}\frac{\partial \omega}{\partial x_j}, 10^{-10}\right)$$

3. Numerical Model

The model developed for the numerical calculations consists of a 3D unstructured grid model with 756,425 tetrahedron elements (Figure 2). The element size of the numerical model varies from 0.01 mm, at the keel's surface, to 4 mm at the boundary surfaces. The elements sizes were optimized in order to obtain a good mesh quality. The mesh quality obtained after the optimization in shown in Figure 1.

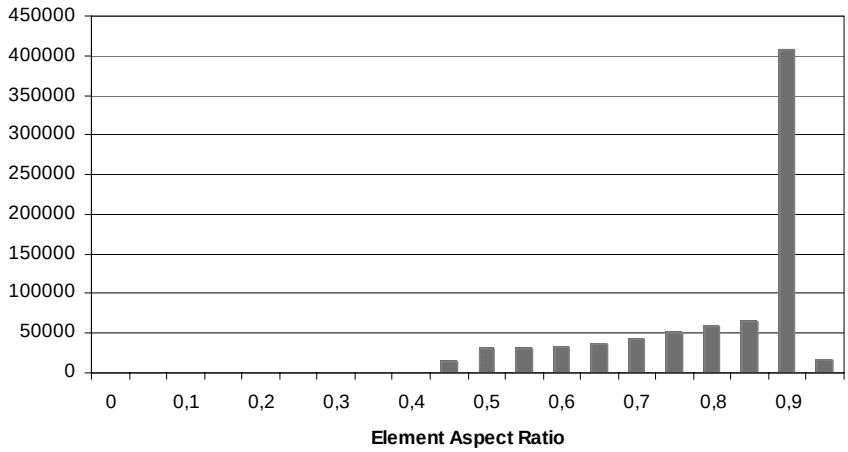

Fig. 1. Histogram of mesh quality values.

The boundary conditions of velocity and turbulence intensity at the model inlet was established based on the results obtained from the experiments with the physical model, as follows:

$$U = 6.0\ \text{m/s}$$
$$u'(\%) = 1.1$$

The flow characteristics of the numerical model were assumed to be isothermal. The temperature was set at 18 ºC, which is the same temperature of air flow during the experiments with the physical model. Due to limitations in measuring the roughness of the physical model, it was assumed the hypothesis of smooth surface for the keel's body.

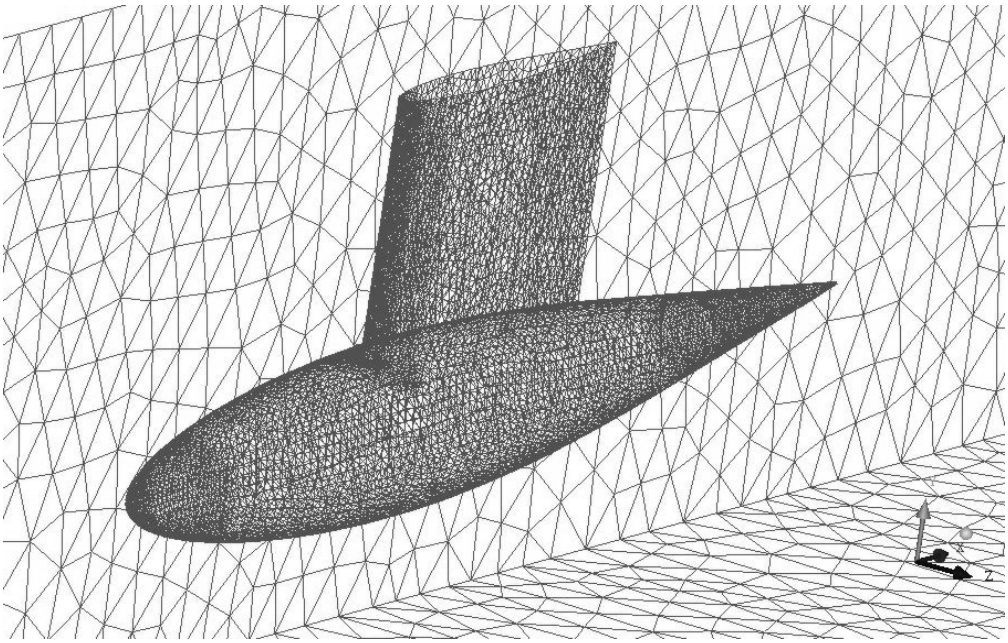

Fig. 2. Numerical model.

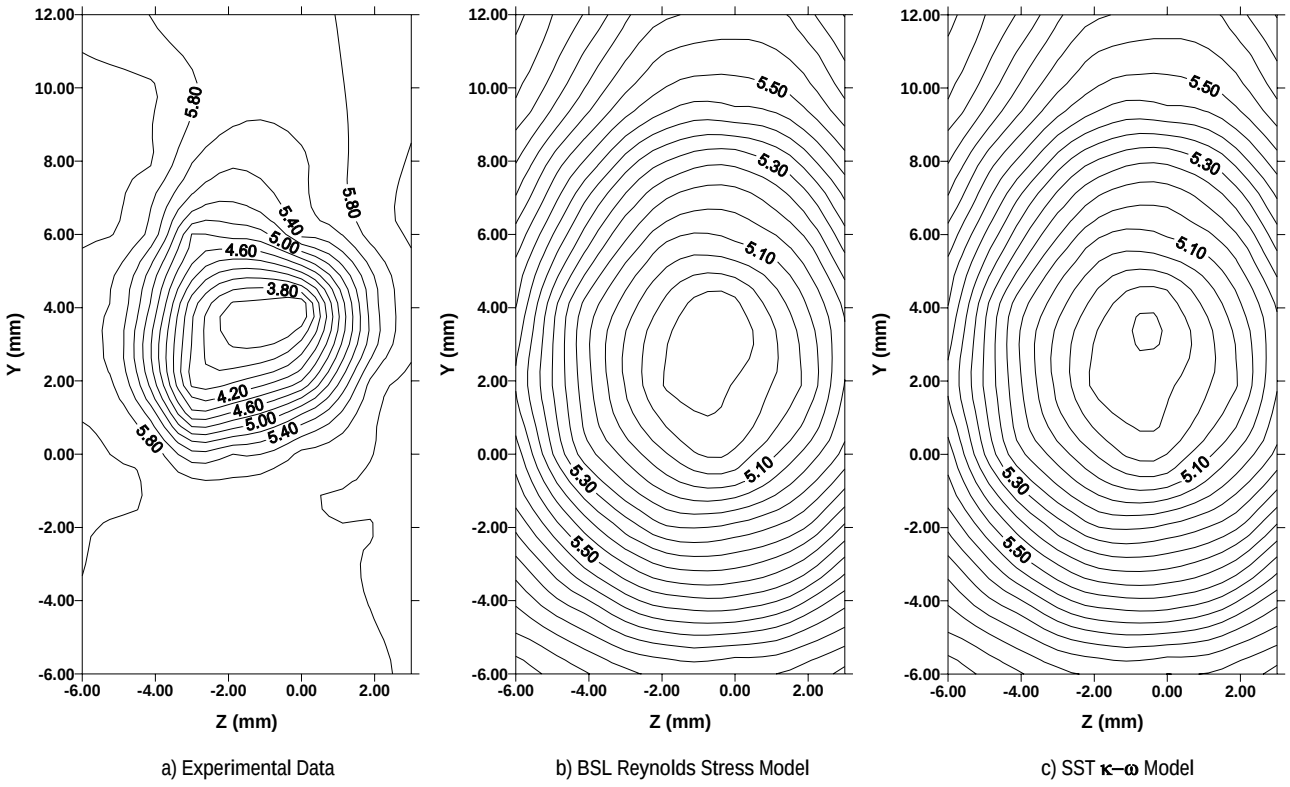

Fig. 3. Velocity distribution at 40 mm after the keel - *U(m/s)*.

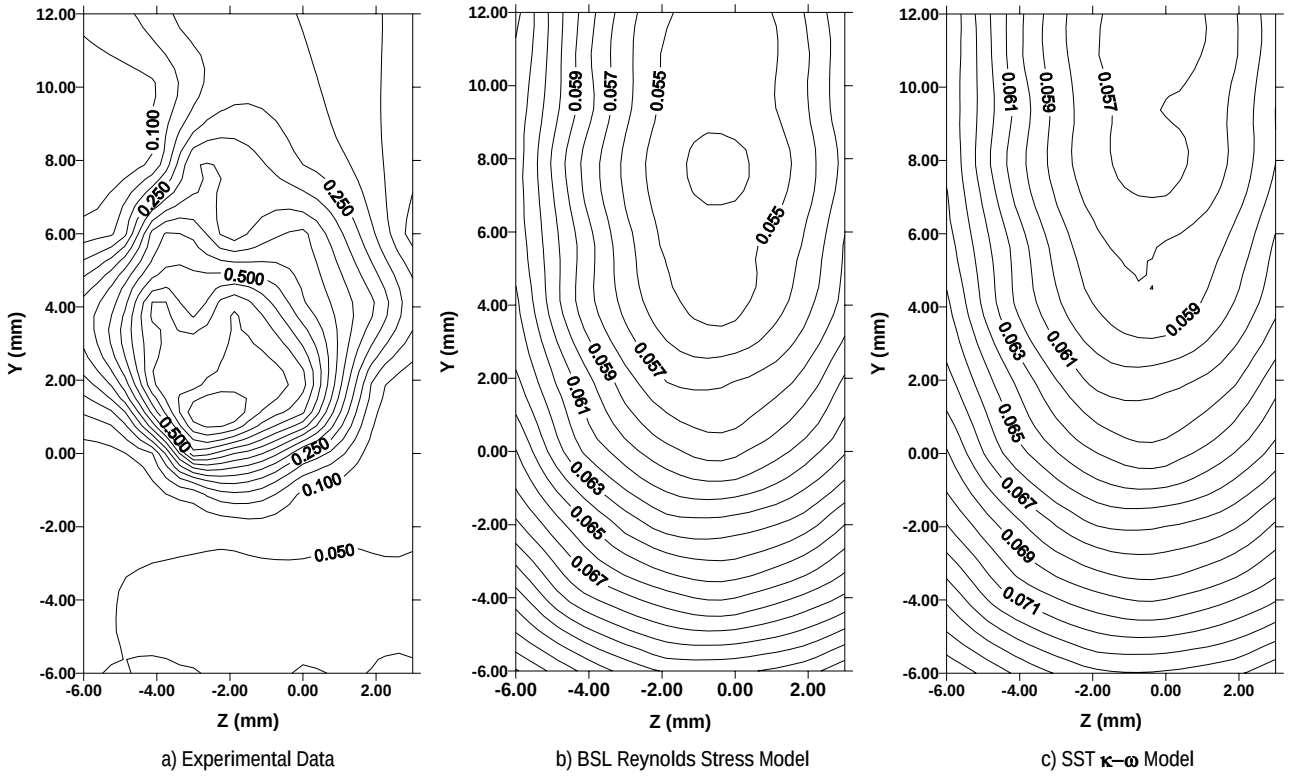

Fig. 4. Fractional turbulence intensity at 40 mm after the keel – *u′*(m/s).

4. Results

In Figures 3 and 4, the results obtained from the numerical calculations are shown in conjunction with the respective experimental data at a position situated 40 mm after the keel. Figure 3 describes the velocity distribution while the fractional turbulence distribution is shown in Figure 4.

One interesting result to be noted is the deflection of the region of higher turbulence action to the left side of the model. This behavior results from a misalignment in the physical model. After a detailed verification of the model dimensions it was observed that it is 0.5 degree inclined to the right and 1.0 degree up in down way direction. This misalignment, unfortunately, could not be removed, as it is a result of the construction of the model. As can be seen, this influence of the misalignment was reproduced on the numerical simulation model. As Figure 3 shows, both the Y-deviation and the Z-deviation were quite similar to those observed with the physical model.

However, a significant difference between the numerical and experimental values of mean velocity can be noted. In particular, the experimental data show a higher velocity gradient than that predicted by the numerical simulations. The results obtained from both numerical models are quite similar in this aspect, which means that both models were unable to predict accurately the behavior of the velocity field after the keel's body. One possible explanation for this discrepancy between numerical and experimental results may be fact that the surface of the keel was assumed to be smooth for the numerical computations. Although, there is no doubt about the influence of the adoption of the hypothesis of smooth surface on the downstream flow field, qualitative investigations based on representative surface roughness values indicate that its effect is not that expressive in the wake of the keel, as shown in Figure 3.

The results obtained for turbulence intensity can contribute to explain the discrepancy between the experimental and numerical velocity fields. As can be noted in Figure 4, the turbulence intensity predicted by the numerical model is much lower than that measured in the real flow field. The difference is about one order of magnitude in the region of higher velocity gradients. The results in the regions of lower velocity gradients show a better agreement with the experimental data, as can be seen for $Y > 8{,}0$ mm and $Y < -2{,}0$ mm.

The remarkable difference in the region of higher velocity gradients indicates that the numerical models were unable to predict the turbulence in the flow around the bulb of the keel. One possible reason for this result is that the interaction that takes place at the junction region between the vertical part of the keel and the bulb produces complex flow elements that both turbulence models were unable to predict.

5. Conclusions

The present work has been successful in provide valuable data for the validation of numerical codes that aim at furnishing realistic engineering predictions for flows downstream of a keel. It is shown that a better prediction of the complex flow elements generated at the junction region between the keel and the bulb is necessary. Particularly, improvements have to be made for the achievement of the right turbulence values in the flow field around the bulb. In this sense, a higher accuracy, at the level of the discretization of flow field as well as in the turbulence models adopted, is required in order to achieve improved numerical results.

*Acknowledgements.*APSF is grateful to the Brazilian National Research Council (CNPq) for the award of a research fellowship (Grant No 304919/2003-9). The work was financially supported by CNPq through Grant No 472215/2003-5 and by the Rio de Janeiro Research Foundation (FAPERJ) through Grants E-26/171.198/2003 and E-26/152.368/2002. RMBC benefited from a M.Sc. scholarship from CAPES. MFOFL received an I.C. scholarship from CNPq.

6. References

Barberis, D., Molton, P. and Malaterre, T., 1998, Control of 3D turbulent boundary layer separation caused by a wing-body junction, Exp. Therm. Fluid Sci. AIAA J., 16, 54-63.

Cummings, R. M. and Simpson, R., 1992, Flow past a wing body junction: experimental evaluation of turbulence models, AIAA J., 30, 873-881.

Davenport, W. J., Forsythe, J. R., Morton, S. A. and Squires, K. D, 2003, Computational challenges in high angle of attack flow prediction, Progress Aero. Sciences, 39, 369-384.

Gatski, T. B.and Jongen, T., 2000, Nonlinear eddy viscosity and algebraic stress models for solving complex turbulen flows, Progress. Aero. Sciences, 36, 655-682.

Ölçmen, M. S. and Simpson, R., 1996, Experimental transport-rate budgets in complex three-dimensional turbulent flows at a wing/body junction, AIAA-96-2035.

Ölçmen, M. S. and Simpson, R., 1997, Experimental evaluation of turbulence diffusion models in complex 3D-flows near a wing/body junction, AIAA-97-0650.

Parneix, S. Durbin, P. A. and Behia, M., 1998, Computation of 3d turbulent boundary layers using the v2-f model, Flow Turbul. Combust., 60, 19-46.

Simpson, R., 2001, Junction Flows, Annu. Rev. Fluid Mechanics, 33, 415-443.